

# Recovery of Soil Moisture Active Passive (SMAP) Instrument's Active Measurements via Coupled Dictionary Learning

Konstantina Fotiadou<sup>1,2</sup>, Grigorios Tsagkatakis<sup>1</sup>, Mahta Moghaddam<sup>3</sup>, Panagiotis Tsakalides<sup>1,2</sup>

<sup>1</sup> ICS- Foundation for Research and Technology - Hellas (FORTH), Crete, Greece

<sup>2</sup> Department of Computer Science, University of Crete, Greece

<sup>3</sup> Electrical Engineering Department, University of Southern California (USC), Los Angeles, CA, USA

## Abstract

NASA's Soil Moisture Active Passive (SMAP) satellite mission combines a passive L-band radiometer and an active Synthetic Aperture Radar (SAR) instrument in order to monitor the near-surface soil moisture and freeze-thaw states globally, with a revisit frequency of 2-3 days. SMAP provides three soil moisture products: a high-resolution from the radar, a low-resolution from the radiometer, and an intermediate-resolution from the fusion of the radar and radiometer measurements. Unfortunately, SMAP's SAR instrument halted its transmissions after a short operating period. In order to address this limitation, we introduce a novel post-acquisition computational technique aiming to synthesize the active measurements of SMAP, by exploiting the mathematical frameworks of Sparse Representations and Dictionary Learning. We propose a coupled dictionary learning model which considers joint feature spaces, composed of active and passive images, in order to recover the missing active measurements. We formulate our coupled dictionary learning problem within the context of the Alternating Direction Method of Multipliers. Our experimental results demonstrate the ability of the proposed approach to reconstruct the active measurements, achieving better performance compared to state-of-the-art coupled dictionary learning techniques.

## Introduction

The Soil Moisture Active Passive (SMAP) instrument [1, 2] constitutes an environmental research observatory that provides measurements of the land surface soil moisture [3]. SMAP acquires space-based hydrosphere state measurements in order to estimate the global water fluxes at the land surface, to enhance the weather and climate forecast capabilities, and to define processes that link the terrestrial water, energy, and carbon cycles. The instrument's architecture consists of an L-band radiometer (passive instrument), with a 1.41 GHz frequency, and H, V, and U polarizations; and an L-band radar (active instrument), with 1.26 GHz frequency, and HH, VV, and HV polarizations. Both active and passive instruments share a single feedhorn and parabolic mesh reflector that rotates around the nadir axis providing a scanning antenna beam with a constant incidence angle of approximately  $40^\circ$ . The SMAP satellite has been launched into a 680-km near-polar sun-synchronous orbit within an eight-day repeat cycle, and equator crossings at 6 A.M. and 6 P.M. local time. At this altitude, the antenna scan configuration yields a 1000-km swath, with a 40-km radiometer resolution and 13 km SAR resolution that provides global coverage within three days at the equator and two days at boreal latitudes ( $> 45^\circ N$ ). Consequently, the active

instrument provides high spatial resolution by sacrificing the soil moisture sensitivity, while the passive instrument provides high soil moisture accuracy, with a coarser spatial resolution. The fusion of the active and passive measurements provides both high spatial resolution and high sensing accuracy, in order to retrieve precisely both the soil moisture and the freeze-thaw states. The main objective of SMAP satellite is to provide measurements of the global soil moisture at the top 5 cm of the ground with an error no greater than  $0.04 \text{ cm}^3/\text{cm}^3$  at 10-km spatial resolution, within a three-day average revisit time over the global land area excluding regions of snow and ice, open water, urban areas, and vegetation with total water content greater than  $5 \text{ kg}/\text{m}^2$ . Figure 1 provides an example that illustrates the region of Greece captured by SMAP's SAR and radiometer instruments at 3-km and 36-km resolutions, respectively, along with the fused result at 9-km resolution.

Unfortunately, within a short period of time after the launch of the SMAP satellite, its active instrument (SAR) halted its transmissions. In contrast, the radiometer (passive) instrument still acquires data, valuable to the prediction of the global soil moisture. Obviously, the recovery of SMAP's active measurements is critical for facilitating weather and climate forecasting skills, including the prediction of extreme environmental events such as droughts and floods, providing high impact on the fields of human health and agriculture. Additionally, studies have shown that using measurements from a single instrument results in reduced accuracy in retrieving the soil moisture levels [4, 5].

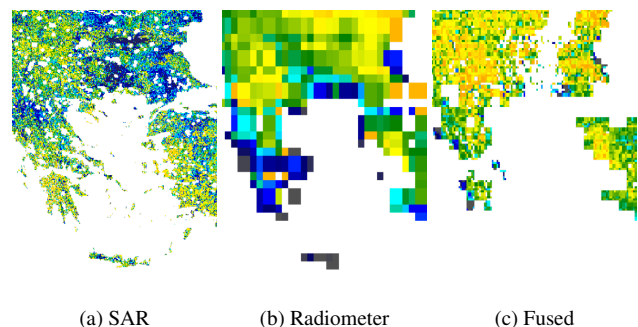


Figure 1: Greece captured by the SMAP satellite: (a) L2\_SM\_A product captured at a 3-km gridding resolution, (b) L2\_SM\_P measurement with a 36-km coarser spatial resolution, (c) L2\_SM\_AP fused result at a 9-km resolution

To address the soil moisture retrieval problem, most state-of-the-art approaches focus on the fusion of the radar and the radiometer measurements. For instance, the authors in [6] propose

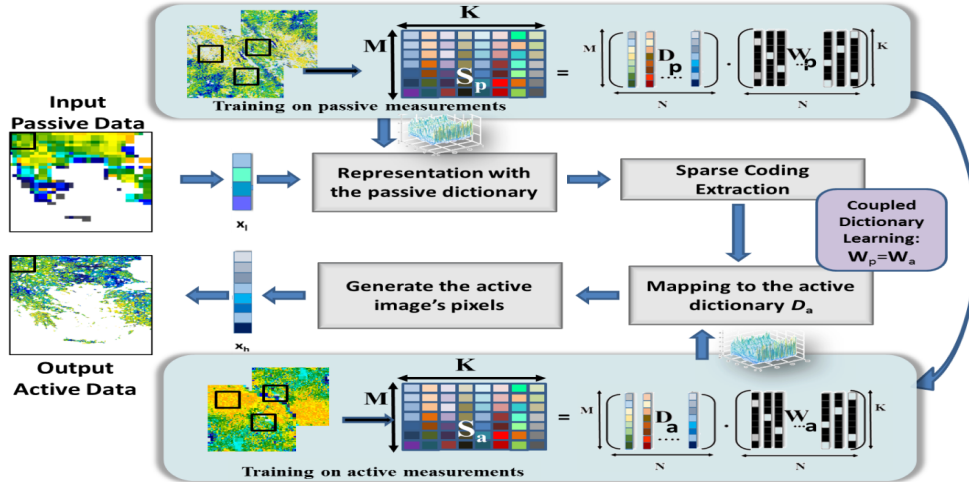


Figure 2: **Block diagram of the proposed scheme:** Overall system block diagram: The system takes as input a passive scene acquired by the SMAP instrument, and produces an estimate of its corresponding active version. During the training phase, multiple active and passive image patches are utilized. Given these patch pairs, a coupled dictionary learning scheme is employed for learning two dictionaries corresponding to the active-passive feature spaces. During the testing phase, passive image patches are mapped to the passive dictionary and the identified sparse coding coefficients are subsequently combined with the active dictionary for synthesizing the reconstruction of the active measurements.

an effective technique that merges the active and passive measurements to create a 9-km soil moisture product. Specifically, they rely on the radar capability to detect high-resolution soil-moisture spatial variability within the coarse-resolution radiometer grid. Their algorithm uses a time-series analysis to determine the slope of the linear relationship between the radar and the radiometer, without requiring the previous satellite overpass measurements to retrieve the current soil-moisture value. The authors in [7] propose a soil moisture retrieval technique using simultaneously both radar and radiometric data in an efficient optimization algorithm that extracts surface soil moisture in vegetation areas. Another interesting technique that combines radar's backscatter and radiometer's brightness temperature measurements for soil moisture estimation is presented in [8]. The authors use physics-based models in order to couple the scattering and emission processes. Additionally, they define a joint cost function that balances the contributions of radar and radiometric measurements, extracting the optimal estimates over a larger range of surface soil moisture. Finally, the authors in [9] present an efficient machine learning scheme, relying on Random Forests, which upscales in-situ soil moisture estimates to the satellite footprints scale of SMAP in order to validate with high accuracy the soil moisture retrieval.

In contrast to the aforementioned techniques, the main objective of this work is the recovery of SMAP instrument's active measurements from its corresponding acquired passive observations. The reconstruction of high resolution SAR estimations will be valuable for subsequent accurate soil moisture retrieval. Using a dual dataset, consisting of active and passive corresponding patch pairs from the time period that both instruments were normally operating, we are able to synthesize the active measurements directly from the currently obtained passive data, and subsequently use them for soil moisture estimation. In order to validate the reconstruction performance, we test our method with a set of active measurements, matched to their corresponding passive ones from the time period that the SAR instrument was func-

tioning. The proposed algorithm capitalizes on the *Sparse Representations* [10] and *Coupled Dictionary Learning* [11–13] frameworks, adhering to the assumption that active image examples can be directly recovered via their corresponding passive versions. Furthermore, we solve the active reconstruction synthesis problem within the Alternating Direction Method of Multipliers optimization framework [14, 15]. Figure 2 illustrates the proposed system's block diagram. To the best of our knowledge, the proposed scheme is the first post-acquisition technique that focuses on the reconstruction of SMAP active measurements.

### Sparse Representations for SMAP's Active Measurements Recovery

In this work, we formulate the problem of SMAP active measurement reconstruction as an inverse imaging problem, considering as input the passive (radiometer) image and seeking to recover its corresponding active (SAR) observation. The recovery of SMAP's active measurements is implemented by capitalizing on the *Sparse Representations* framework [10], according to which, image patches  $\mathbf{x} \in \mathbb{R}^m$ , extracted from active images can be represented as a sparse linear combination of elementary signals encoded in a dictionary matrix,  $\mathbf{D}_a \in \mathbb{R}^{m \times n}$ , generated from a collection of active training image patches. The sparse coding is formulated in a vector  $\mathbf{w}$ , such that  $\mathbf{x} = \mathbf{D}_a \mathbf{w}$ , where  $\|\mathbf{w}\|_0 \leq n$  represents the sparsity assumption. Instead of directly observing the active patches, we observe the corresponding passive patches  $\mathbf{y} \in \mathbb{R}^{m \times n}$  of the input scene. Similarly, patches extracted from passive scenes can be directly mapped onto a dictionary matrix  $\mathbf{D}_p \in \mathbb{R}^{m \times n}$ , constructed by training elements selected from corresponding passive images using a set of sparse vectors. The theory of SR suggests that the sparse coding vectors among the two different representations are the same, and one can recover the active image patches by using the estimated passive sparse coding vectors. As a result, the optimization problem is formulated as:

$$\mathbf{w}^* = \arg \min_{\mathbf{w}} \|\mathbf{s}_p - \mathbf{D}_p \mathbf{w}\|_F^2 + \rho \|\mathbf{w}\|_1 \quad (1)$$

The parameter  $\rho$  stands for the regularization term, while it balances the fidelity of the solution. To obtain the active image patch, the optimal sparse coding  $\mathbf{w}^*$  from (1), is directly projected onto the active dictionary  $\mathbf{D}_\alpha \in \mathbb{R}^{M \times N}$ , to synthesize the active image patch, according to  $\mathbf{s}_\alpha = \mathbf{D}_\alpha \mathbf{w}^*$ . However, the main challenge pertaining to the estimation of the active image patches is related to the proper construction of the dictionary matrices, to simultaneously sparsify both the active and passive measurements. The following paragraph describes in detail the coupled dictionary learning procedure that we propose in this work.

### Coupled Dictionary Learning

Coupled dictionary learning relies on generating a pair of dictionaries which jointly encode the active,  $\mathbf{S}_\alpha$ , and the passive,  $\mathbf{S}_p$ , feature spaces where the signals have sparse representations in terms of the trained dictionaries [16]. The main task is to recover a coupled dictionary pair  $\mathbf{D}_\alpha$  and  $\mathbf{D}_p$  for the spaces  $\mathbf{S}_\alpha$  and  $\mathbf{S}_p$ , respectively [10], and their corresponding sparse codes  $\mathbf{W}_\alpha$  and  $\mathbf{W}_p$ , under the constraint  $\mathbf{W}_\alpha = \mathbf{W}_p$ , by solving the following sparse matrix decomposition problems:

$$\operatorname{argmin}_{\mathbf{D}_\alpha, \mathbf{W}_\alpha} \|\mathbf{D}_\alpha \mathbf{W}_\alpha - \mathbf{S}_\alpha\|_F + \lambda_\alpha \|\mathbf{W}_\alpha\|_1, \|\mathbf{D}_\alpha(:, j)\|_2 \leq 1 \quad (2)$$

$$\operatorname{argmin}_{\mathbf{D}_p, \mathbf{W}_p} \|\mathbf{D}_p \mathbf{W}_p - \mathbf{S}_p\|_F + \lambda_p \|\mathbf{W}_p\|_1, \|\mathbf{D}_p(:, j)\|_2 \leq 1,$$

where  $\lambda_\alpha$  and  $\lambda_p$  denote the sparsity regularization parameters, for the active and the passive feature spaces, respectively. A straightforward approach is to concatenate the coupled feature spaces and use a common sparse representation. Consequently, the coupled dictionary learning problem is converted into a single dictionary learning problem that can be efficiently solved via existing algorithms, such as the K-SVD [17, 18]. However, a major limitation of single dictionary learning strategies is their inability to guarantee that the same sparse coding can be separately utilized in both active and passive representations.

To overcome this limitation, we propose a computationally efficient coupled dictionary learning technique, based on the Alternating Direction Method of Multipliers (ADMM) scheme [14, 15], that converts the constrained dictionary learning problem in (2), into an unconstrained version which can be efficiently solved via alternating minimizations. To apply the ADMM technique in our coupled dictionary learning scheme, we reformulate the minimization problem posed in (2) as:

$$\min_{\mathbf{D}_\alpha, \mathbf{W}_\alpha, \mathbf{D}_p, \mathbf{W}_p} \|\mathbf{S}_\alpha - \mathbf{D}_\alpha \mathbf{W}_\alpha\|_F^2 + \|\mathbf{S}_p - \mathbf{D}_p \mathbf{W}_p\|_F^2 + \quad (3)$$

$$\lambda_p \|\mathbf{Q}\|_1 + \lambda_\alpha \|\mathbf{P}\|_1, \text{ subject to: } \mathbf{P} = \mathbf{W}_\alpha, \mathbf{Q} = \mathbf{W}_p,$$

$$\mathbf{W}_\alpha = \mathbf{W}_p, \|\mathbf{D}_\alpha(:, i)\|_2 \leq 1, \|\mathbf{D}_p(:, i)\|_2 \leq 1$$

The ADMM technique takes into account the separate structure of each variable in (3), relying on the minimization of its augmented Lagrangian function:

$$\begin{aligned} \mathcal{L}(\mathbf{D}_\alpha, \mathbf{D}_p, \mathbf{W}_\alpha, \mathbf{W}_p, \mathbf{P}, \mathbf{Q}, Y_1, Y_2, Y_3) = & \frac{1}{2} \|\mathbf{D}_\alpha \mathbf{W}_\alpha - \mathbf{S}_\alpha\|_F^2 \\ & + \frac{1}{2} \|\mathbf{D}_p \mathbf{W}_p - \mathbf{S}_p\|_F^2 + \lambda_\alpha \|\mathbf{P}\|_1 + \lambda_p \|\mathbf{Q}\|_1 + \langle Y_1, \mathbf{P} - \mathbf{W}_\alpha \rangle \\ & + \langle Y_2, \mathbf{Q} - \mathbf{W}_p \rangle + \langle Y_3, \mathbf{W}_\alpha - \mathbf{W}_p \rangle + \frac{c_1}{2} \|\mathbf{P} - \mathbf{W}_\alpha\|_F^2 \\ & + \frac{c_2}{2} \|\mathbf{Q} - \mathbf{W}_p\|_F^2 + \frac{c_3}{2} \|\mathbf{W}_\alpha - \mathbf{W}_p\|_F^2, \end{aligned} \quad (4)$$

where  $\mathbf{Y}_1$ ,  $\mathbf{Y}_2$ , and  $\mathbf{Y}_3$  stand for the Lagrange multiplier matrices, while  $c_1 > 0$ ,  $c_2 > 0$ , and  $c_3 > 0$  denote the step size parameters.

We empirically set the step size parameters to  $c_1 = c_2 = 0.4$  and  $c_3 = 0.8$ . Following the algorithmic strategy of the ADMM scheme, we seek for the stationary point, solving iteratively for each one of the variables, while keeping the others fixed. The overall algorithm for learning the coupled dictionaries is summarized in **Algorithm 1**.

---

#### Algorithm 1 Coupled Dictionary Learning

---

**Input:** training examples  $\mathbf{S}_c$  and  $\mathbf{S}_n$ , iterations:  $K$ , step size parameters:  $c_1, c_2, c_3$ .

**Initialization of the Dictionaries:** Random selection of the columns of  $\mathbf{S}_\alpha$  and  $\mathbf{S}_p$ ; Initialization of Lagrange multiplier matrices:  $\mathbf{Y}_1 = \mathbf{Y}_2 = \mathbf{Y}_3 = \mathbf{0}$ .

**for**  $k = 1, \dots, K$  **do**

1. Update  $\mathbf{W}_\alpha$  and  $\mathbf{W}_p$ :

$$\mathbf{W}_\alpha = (\mathbf{D}_\alpha^T \mathbf{D}_\alpha + c_1 \mathbf{I} + c_3 \mathbf{I})^{-1} \cdot (\mathbf{D}_\alpha^T \mathbf{S}_\alpha + Y_1 - Y_3 + c_1 \mathbf{P} + c_3 \mathbf{W}_p)$$

$$\mathbf{W}_p = (\mathbf{D}_p^T \mathbf{D}_p + c_2 \mathbf{I} + c_3 \mathbf{I})^{-1} \cdot (\mathbf{D}_p^T \mathbf{S}_p + Y_2 + Y_3 + c_2 \mathbf{Q} + c_3 \mathbf{W}_\alpha)$$

2. Update  $\mathbf{P}$  and  $\mathbf{Q}$ :

$$\mathbf{P} = S_{\lambda_\alpha} \left( \mathbf{W}_\alpha - Y_1 / c_1 \right)$$

$$\mathbf{Q} = S_{\lambda_p} \left( \mathbf{W}_p - Y_2 / c_2 \right),$$

3. **for**  $j = 1, \dots, N$  **do**

• Update  $\phi_c$  and  $\phi_n$ :

$$\phi_\alpha = \mathbf{W}_\alpha(j, :) \mathbf{W}_\alpha(j, :)^T$$

$$\phi_p = \mathbf{W}_p(j, :) \mathbf{W}_p(j, :)^T$$

• Update the dictionaries  $\mathbf{D}_\alpha$  and  $\mathbf{D}_p$ :

$$\mathbf{D}_\alpha^{(k+1)}(:, j) = \mathbf{D}_\alpha^{(k)}(:, j) + (\mathbf{S}_\alpha \mathbf{W}_\alpha(j, :)) / (\phi_\alpha + \delta)$$

$$\mathbf{D}_p^{(k+1)}(:, j) = \mathbf{D}_p^{(k)}(:, j) + (\mathbf{S}_p \mathbf{W}_p(j, :)) / (\phi_p + \delta)$$

**end**

• Normalize  $\mathbf{D}_\alpha$  and  $\mathbf{D}_p$  between  $[0, 1]$

• Update Lagrange multiplier matrices  $Y_1, Y_2$  and  $Y_3$ :

$$Y_1^{(k+1)} = Y_1^{(k)} + c_1 (\mathbf{P} - \mathbf{W}_\alpha)$$

$$Y_2^{(k+1)} = Y_2^{(k)} + c_2 (\mathbf{Q} - \mathbf{W}_p)$$

$$Y_3^{(k+1)} = Y_3^{(k)} + c_3 (\mathbf{W}_\alpha - \mathbf{W}_p)$$

**end**

---

### Experimental Setup

In this paragraph, we evaluate the performance of the proposed ADMM coupled dictionary learning scheme when applied to the recovery of SMAP instrument's active (SAR) measurements. In this paper, we worked with SMAP's Level-2 products. Specifically, we considered L2.SM.A active (SAR) measurements and their corresponding L2.SM.P passive (Radiometer) observations. The gridding resolution of the L2.SM.A product is 3 km, while the coarser resolution of the L2.SM.P passive product is 36 km. In terms of spatial resolution, both the active and passive images are of size  $(1134 \times 1034)$  pixels. To validate the reconstruction performance, we measured both the Peak Signal to Noise Ratio (PSNR) and the Root Mean Square Error (RMSE) metrics, between the reconstructed and the ground truth SAR measurements. The PSNR error metric between the original and the reconstructed scene is defined as:

$$PSNR = 10 \times \log_{10} \left( \frac{MAX^2 I}{MSE} \right), \quad (5)$$

where the mean square error is defined as:

$$MSE = \frac{1}{m \times n} \sum_{i=0}^{m-1} \sum_{j=0}^{n-1} [I(i, j) - \hat{I}(i, j)]^2 \quad (6)$$

Specifically,  $m \times n$  stand for the spatial dimensions of the images,  $I$  denotes the ground truth active scene, while  $\hat{I}$  represents the reconstructed active observation.  $MAX_I$  denotes the maximum possible pixel value of the scene. Moreover, each active reconstruction is compared against the corresponding ground truth active measurement in terms of the *Structural Similarity Index Metric* [19], a psychophysically modeled error metric defined as:

$$SSIM(x, y) = \frac{(2\mu_x\mu_y + c_1) \cdot (2\sigma_{xy} + c_2)}{(\mu_x^2 + \mu_y^2 + c_1) \cdot (\sigma_x^2 + \sigma_y^2 + c_2)}, \quad (7)$$

where  $\mu$  and  $\sigma$  stand for the mean value and the standard deviation, respectively. Finally, we measured the absolute difference [9] between the reconstructed and the ground truth active measurements. The absolute difference is widely used in soil moisture retrieval problems. Relatively small values of the absolute difference index indicate both high reconstruction quality and high soil moisture retrieval accuracy.

During the coupled dictionary training phase, one pair of dictionaries was prepared, corresponding to the active and passive measurements. Specifically, we utilized 100,000 randomly selected  $(3 \times 3)$  patch pairs from corresponding active-passive training images. Additionally, in order to study the sensitivity of the proposed algorithm, we evaluated the reconstruction performance of the coupled trained dictionaries when different patch sizes were used. Figure 3 provides the PSNR (dB) values for the reconstruction of the active measurements of California, when  $(3 \times 3)$ ,  $(5 \times 5)$ ,  $(7 \times 7)$ , and  $(9 \times 9)$  patch sizes were used. The number of the representative dictionary atoms that we utilized in our proposed ADMM coupled dictionary learning scheme was set to 512, balancing the computational cost with the robustness of the representation. As we may observe, the optimal reconstruction performance is achieved when we use a small patch size  $(3 \times 3)$ , with 2 pixels overlapping factor. We observe, that as we increase the patch size, the reconstruction quality is degraded.

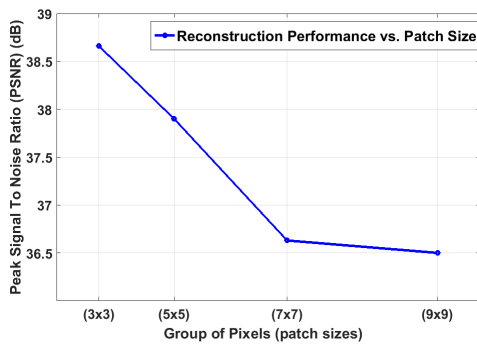


Figure 3: California's SAR measurement reconstruction. In this figure we examine the reconstruction performance of the active measurement, when different patch sizes were used for both the coupled dictionary training and the reconstruction phases. We observe that the best performance is achieved when we use a small patch size, of  $(3 \times 3)$ , with 2 overlapping parameter between adjacent pixels.

Similarly, we investigated the performance of the proposed ADMM scheme as a function of dictionary size. Specifically, we have experimented with 256, 512, 1024, and 2048 dictionary

atoms. In Figure 4 we illustrate the reconstruction performance in terms of the PSNR metric when the aforementioned numbers of dictionary atoms were used. As we may observe, the best performance is achieved when we use 512 dictionary atoms. In this simulation, the patch size is set to  $(3 \times 3)$ , with a 2 overlapping factor among adjacent pixels.

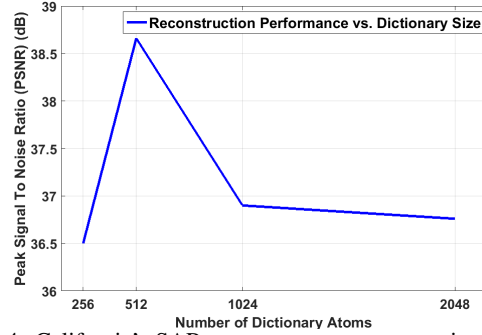


Figure 4: California's SAR measurement reconstruction. In this figure we examine the reconstruction performance of the active measurement as a function of the number of dictionary atoms used. As we may observe, the best performance is achieved when we use 512 dictionary atoms. Additionally, as the dictionary size increases above 512, the reconstruction quality decreases.

In order to quantify the performance of the proposed ADMM coupled dictionary learning scheme, we investigate the empirical convergence behavior of the Augmented Lagrangian function, and the coupled dictionaries. Figure 5 depicts the normalized reconstruction error for the active-passive pair of dictionaries and the Augmented Lagrangian function as a function of the number of iterations. We observe that both the coupled dictionaries and the augmented Lagrangian function converge into a stationary point, after a small number of iterations.

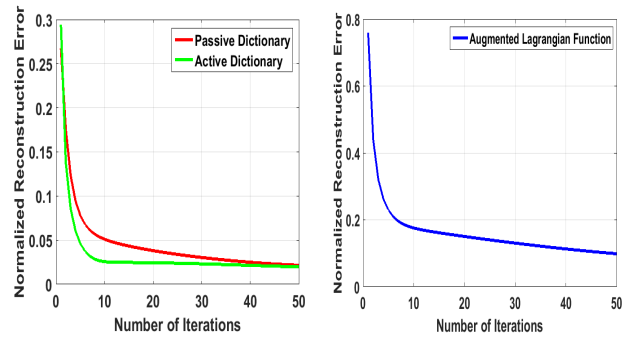
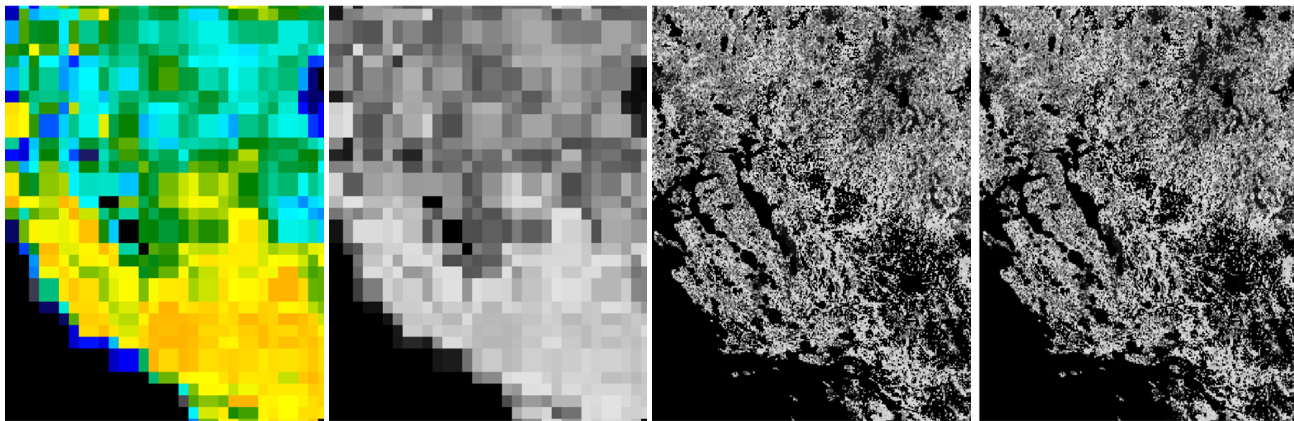


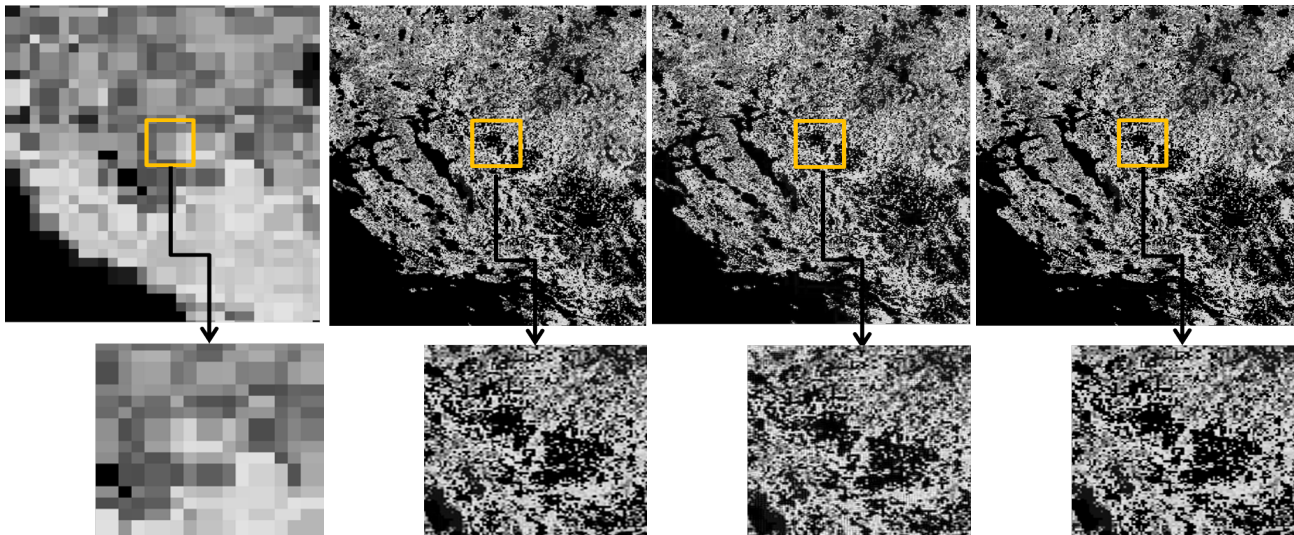
Figure 5: (a) Convergence Behaviour of the ADMM coupled dictionary learning Algorithm, (b) Convergence of the augmented Lagrangian function. The number of dictionary atoms was fixed to 512, while we used a  $(3 \times 3)$  patch size. We observe that the coupled dictionaries and the augmented Lagrangian function converge into a stationary point after approximately 10 iterations.

## Simulation Results

Figure 6 illustrates an exemplary active reconstruction of California's region using the proposed ADMM coupled dictionary



(a) Input Passive California (RGB) (b) Input Passive California (c) Ground Truth Active (d) Reconstructed Active, SSIM: **0.96**  
 Figure 6: California's Region Active Recovery. (a) L2\_SM\_P product in RGB color-map, (b) L2\_SM\_P product in gray-scale, (c) L2\_SM\_A product's ground truth active measurements, (d) ADMM recovery of the active measurements. As we may observe, the proposed sparsity-based technique is able to reconstruct accurately the missing SAR (active) measurements.



(a) Input Passive California (RGB) (b) Ground Truth (c) K-SVD, RMSE: 5.22 (d) Proposed, RMSE: **2.97**  
 Figure 7: California's Region Active Recovery - Comparison with the State-of-the-art. (a) Input L2\_SM\_P passive measurements, (b) Ground Truth L2\_SM\_A active measurements, (c) K-SVD reconstruction of the active measurements (d) ADMM recovery of the active measurements. As we may observe, the proposed algorithm outperforms the state-of-the-art K-SVD technique, both in terms of the evaluation indexes and visually. Additionally, in the zoomed yellow-square regions (depicted on the second row), we illustrate the subtle differences among the compared techniques.

learning scheme. As we may observe, our algorithm is able to reconstruct with great efficiency the corresponding active measurement from this challenging passive observation. In terms of the PSNR evaluation error metric, the proposed technique achieves a similarity index of **0.96**, validating the high similarity of the recovered active observation with respect to the ground truth active measurement.

Another interesting reconstruction is presented in figure 7, where we demonstrate the performance of the proposed ADMM coupled dictionary learning algorithm, versus the state-of-the-art K-SVD dictionary learning scheme. Although the K-SVD coupled algorithm produces faithful approximations of the ground truth active measurement, the proposed ADMM technique synthesizes high quality SAR observations without introducing noise

effects. Quantitatively, the proposed SCDL scheme outperforms the K-SVD comparable technique, in terms of the evaluation metrics, achieving a PSNR value of **38.66** dB, in contrast to the K-SVD that achieves 33.77 dB. Additionally, in terms of RMSE, the proposed algorithm achieves **2.97**, in contrast with the 5.22 of the K-SVD technique. Similarly, measuring the absolute difference among the comparable techniques, we observe that the proposed scheme achieves a smaller absolute difference of **1.26**, in contrast with the K-SVD recovery that achieves 1.45. Consequently, the smallest absolute difference indicates a more representative approximation of the ground truth active measurement. Finally, in terms of the structural similarity index (SSIM), the proposed ADMM coupled dictionary learning algorithm achieves a 0.96 SSIM index, compared to the 0.89 of the K-SVD technique.

## Conclusions and Future Work

In this paper, we developed a novel technique that tackles the problem of recovering SMAP instrument's active measurements. The reported experimental results suggest that Sparse Representations and Coupled Dictionary Learning are powerful tools, able to reconstruct SAR measurements from their corresponding passive observations. Additionally, we observed that the proposed reconstruction scheme works successfully with these extreme coarse resolution passive observations. The developed coupled dictionary learning scheme can be efficiently used in satellite instruments, where knowledge transfer is required. In our future work, we aim to exploit the ADMM coupled dictionary learning scheme in order to combine in-situ soil moisture estimates with brightness and temperature satellite measurements from radiometer's instrument of the SMAP satellite, in order to provide accurate predictions concerning the global soil moisture.

## Acknowledgments

This work was funded by the DEDALE project contract no. 665044 within the H2020 Framework Program of the European Commission.

## References

- [1] Dara Entekhabi, Eni G Njoku, Peggy E O'Neill, Kent H Kellogg, Wade T Crow, Wendy N Edelman, Jared K Entin, Shawn D Goodman, Thomas J Jackson, Joel Johnson, et al., "The soil moisture active passive (smap) mission," *Proceedings of the IEEE*, vol. 98, no. 5, pp. 704–716, 2010.
- [2] Dara Entekhabi, Eni Njoku, Peggy O'Neill, Michael Spencer, Tom Jackson, Jared Entin, Eastwood Im, and Kent Kellogg, "The soil moisture active/passive mission (smap)," in *Geoscience and Remote Sensing Symposium, 2008. IGARSS 2008. IEEE International*. IEEE, 2008, vol. 3, pp. III–1.
- [3] Rocco Panciera, Jeffrey P Walker, Thomas J Jackson, Douglas A Gray, Mihai A Tanase, Dongryeol Ryu, Alessandra Moneris, Heath Yardley, Christoph Rudiger, Xiaoling Wu, et al., "The soil moisture active passive experiments (smapex): Toward soil moisture retrieval from the smap mission," *IEEE transactions on geoscience and remote sensing*, vol. 52, no. 1, pp. 490–507, 2014.
- [4] Eni G Njoku and Dara Entekhabi, "Passive microwave remote sensing of soil moisture," *Journal of hydrology*, vol. 184, no. 1-2, pp. 101–129, 1996.
- [5] Fawwaz T Ulaby, Pascale C Dubois, and Jakob Van Zyl, "Radar mapping of surface soil moisture," *Journal of Hydrology*, vol. 184, no. 1-2, pp. 57–84, 1996.
- [6] Narendra N Das, Dara Entekhabi, and Eni G Njoku, "An algorithm for merging smap radiometer and radar data for high-resolution soil-moisture retrieval," *IEEE Transactions on Geoscience and Remote Sensing*, vol. 49, no. 5, pp. 1504–1512, 2011.
- [7] Ruzbeh Akbar and Mahta Moghaddam, "A radar-radiometer surface soil moisture retrieval algorithm for smap," in *Geoscience and Remote Sensing Symposium (IGARSS), 2013 IEEE International*. IEEE, 2013, pp. 1095–1098.
- [8] Ruzbeh Akbar and Mahta Moghaddam, "Radar-radiometer soil moisture estimation with joint physics and adaptive regularization in support of smap," in *Geoscience and Remote Sensing Symposium (IGARSS), 2014 IEEE International*. IEEE, 2014, pp. 3634–3637.
- [9] Daniel Clewley, Jane B Whitcomb, Ruzbeh Akbar, Agnelo R Silva, Aaron Berg, Justin R Adams, Todd Caldwell, Dara Entekhabi, and Mahta Moghaddam, "A method for up-scaling in situ soil moisture measurements to satellite footprint scale using random forests," *IEEE Journal of Selected Topics in Applied Earth Observations and Remote Sensing*, 2017.
- [10] Michael Elad, "Prologue," in *Sparse and Redundant Representations*, pp. 3–15. Springer, 2010.
- [11] Jianchao Yang, John Wright, Thomas S Huang, and Yi Ma, "Image super-resolution via sparse representation," *IEEE transactions on image processing*, vol. 19, no. 11, pp. 2861–2873, 2010.
- [12] Li He, Hairong Qi, and Russell Zaretzki, "Beta process joint dictionary learning for coupled feature spaces with application to single image super-resolution," in *Proceedings of the IEEE Conference on Computer Vision and Pattern Recognition*, 2013, pp. 345–352.
- [13] Min Guo, Hongyan Zhang, Jiayi Li, Liangpei Zhang, and Huanfeng Shen, "An online coupled dictionary learning approach for remote sensing image fusion," *IEEE Journal of Selected Topics in Applied Earth Observations and Remote Sensing*, vol. 7, no. 4, pp. 1284–1294, 2014.
- [14] Stephen Boyd, Neal Parikh, Eric Chu, Borja Peleato, and Jonathan Eckstein, "Distributed optimization and statistical learning via the alternating direction method of multipliers," *Foundations and Trends® in Machine Learning*, vol. 3, no. 1, pp. 1–122, 2011.
- [15] Mingyi Hong, Zhi-Quan Luo, and Meisam Razaviyayn, "Convergence analysis of alternating direction method of multipliers for a family of nonconvex problems," *SIAM Journal on Optimization*, vol. 26, no. 1, pp. 337–364, 2016.
- [16] Konstantina Fotiadou, Grigorios Tsagkatakis, and Panagiotis Tsakalides, "Spectral resolution enhancement of hyperspectral images via sparse representations," in *Proceedings Proc. Computational Imaging, IS&T Int. Symposium on Electronic Imaging*, 2016.
- [17] Michal Aharon, Michael Elad, and Alfred Bruckstein, "K-svd: An algorithm for designing overcomplete dictionaries for sparse representation," *IEEE Transactions on signal processing*, vol. 54, no. 11, pp. 4311–4322, 2006.
- [18] Michal Aharon, Michael Elad, and Alfred M Bruckstein, "K-svd and its non-negative variant for dictionary design," in *Optics & Photonics 2005*. International Society for Optics and Photonics, 2005, pp. 591411–591411.
- [19] Zhou Wang, Alan C Bovik, Hamid R Sheikh, and Eero P Simoncelli, "Image quality assessment: from error visibility to structural similarity," *IEEE transactions on image processing*, vol. 13, no. 4, pp. 600–612, 2004.